

Magnetoelastic studies of $\text{Nd}_{0.75}\text{Dy}_{0.25}\text{Fe}_3(\text{BO}_3)_4$ in the external magnetic field: Magnetic phase transitions

Cite as: Low Temp. Phys. **39**, 936 (2013); <https://doi.org/10.1063/1.4826082>

Submitted: 31 May 2013 . Accepted: 04 October 2013 . Published Online: 26 November 2013

G. A. Zvyagina, K. R. Zhekov, I. V. Bilych, A. A. Zvyagin, I. A. Gudim, V. L. Temerov, and E. V. Eremin



View Online



Export Citation



CrossMark

ARTICLES YOU MAY BE INTERESTED IN

[The condition for a large magnetoresistance effect in perovskite cobaltites](#)

Low Temperature Physics **39**, 948 (2013); <https://doi.org/10.1063/1.4830262>

[Magnetolectric and magnetoelastic properties of rare-earth ferrobates](#)

Low Temperature Physics **36**, 511 (2010); <https://doi.org/10.1063/1.3457390>

[Vortex pattern and differential conductance in hole underdoped high-temperature superconductors with competing d-wave and antiferromagnetic orders](#)

Low Temperature Physics **39**, 923 (2013); <https://doi.org/10.1063/1.4826081>

LOW TEMPERATURE TECHNIQUES
OPTICAL CAVITY PHYSICS
MITIGATING THERMAL
& VIBRATIONAL NOISE

[DOWNLOAD THE WHITE PAPER](#)

downloads.montanainstruments.com/optical_cavities

MONTANA INSTRUMENTS
COLD SCIENCE MADE SIMPLE



LOW-TEMPERATURE MAGNETISM

Magnetoelastic studies of $\text{Nd}_{0.75}\text{Dy}_{0.25}\text{Fe}_3(\text{BO}_3)_4$ in the external magnetic field: Magnetic phase transitions

G. A. Zvyagina,^{a)} K. R. Zhekov, I. V. Bilych, and A. A. Zvyagin

B. I. Verkin Institute for Low Temperature Physics and Engineering of the National Academy of Sciences of Ukraine, 47 Lenin Ave., Kharkov 61103, Ukraine

I. A. Gudim, V. L. Temerov, and E. V. Eremin

L. V. Kirensky Institute of Physics, Siberian Branch of the Russian Academy of Sciences, Krasnoyarsk 660036, Russia

(Submitted May 31, 2013)

Fiz. Nizk. Temp. **39**, 1202–1214 (November 2013)

We report on results of sound-velocity and sound-attenuation measurements in the $\text{Nd}_{0.75}\text{Dy}_{0.25}\text{Fe}_3(\text{BO}_3)_4$ in external magnetic fields up to 5 T, applied along several directions with respect to crystallographic axes, and at temperatures down to 1.7 K. The experimental data are analyzed with a microscopic theory based on exchange-striction coupling and phenomenological theory resulting in a qualitative agreement between theoretical results and experimental data. © 2013 AIP Publishing LLC. [<http://dx.doi.org/10.1063/1.4826082>]

1. Introduction

During the last decades multiferroic systems came into the focus of solid-state physics. Crystals belonging to the family $\text{ReFe}_3(\text{BO}_3)_4$ ($\text{Re}^{3+} = \text{Y, La-Nd, Sm-Er}$) borates with the trigonal structure (the spatial group $R\bar{3}2$) have interesting optical, magnetic, and magnetoelectric properties. Furthermore, multiferroic effects have been discovered in some of them.¹ That is why this family of crystals is a subject of intensive study nowadays. Their specific magnetic properties are caused by the presence of two types of magnetic ions: iron and rare earth ones. Antiferromagnetic ordering in iron subsystem develops in most of compounds (at the Neel temperature $T_N = 30\text{--}40$ K). A spontaneous and magneto-induced electrical polarization also develops in some of them in the magnetically ordered state. Re^{3+} ions produce the main contribution to the magnetic anisotropy of the ferrobates, while iron ions are in an orbital singlet state and a magnetic anisotropy induced in them can be mostly due to the weak magnetic dipole-dipole interaction. Hence magnetic structures, realized in these crystals, depend on the type of Re^{3+} ion and are very diverse. These compounds can be easy-axis (EA) antiferromagnets (Tb, Dy-based ferrobates), and easy-plane (EP) antiferromagnets (Nd, Sm-based ferrobates), or they can spontaneously transform from the EP to an EA state (Gd, Ho-based ferrobates). In binary compounds of the type $\text{Nd}_{1-x}\text{Dy}_x\text{Fe}_3(\text{BO}_3)_4$ contributions of the Re^{3+} ions to the magnetic anisotropy can have the competitive character with one another and spontaneous reorientation from the EP to the EA state is possible.

Indeed, in Ref. 2, it was reported the discovery of the spontaneous spin reorientation in the compound $\text{Nd}_{0.75}\text{Dy}_{0.25}\text{Fe}_3(\text{BO}_3)_4$. According to Ref. 2, the antiferromagnetic structure with the magnetic moments oriented in the basic plane (EP anisotropy), which is formed in the crystal below $T_N = 32$ K, transforms spontaneously at $T_R = 25$ K to an

EA magnetic configuration. Studies of the specific heat, magnetization³ and our magnetoacoustic investigations^{4,5} of $\text{Nd}_{0.75}\text{Dy}_{0.25}\text{Fe}_3(\text{BO}_3)_4$ crystal have shown that the restructuring of its magnetic structure does not reduce to a simple superposition of the features characteristic of the $\text{NdFe}_3(\text{BO}_3)_4$ and $\text{DyFe}_3(\text{BO}_3)_4$. In this compound we have detected new phase transitions (PTs): the spontaneous PT (with the temperature at $T_{\text{cr1}} = 16$ K), and the one, induced by the external magnetic field, applied along the trigonal crystal axis C_3 , and applied in the basic plane. We have constructed the H - T phase diagrams for the cases $\mathbf{H} \parallel C_3$, $\mathbf{H} \parallel C_2$ and $\mathbf{H} \perp C_2$, and have detected that this compound exhibited several PT lines and, correspondingly, several magnetic phases. Magnetic structures that are implemented in these phases are not defined yet. Although, based on data from the experiments,²⁻⁵ it can be assumed that in the absence of the magnetic field the most of the low-temperature phase (below $T_{\text{cr1}} = 16$ K) corresponds to the EA configuration. Phase, which is realized in the range $25 \text{ K} < T < T_N$, was supposed to be the EP one.² Magnetic configuration in the range $16 \text{ K} < T < 25 \text{ K}$ is now the subject of debate. In Refs. 4 and 5, we have suggested that the crystal $\text{Nd}_{0.75}\text{Dy}_{0.25}\text{Fe}_3(\text{BO}_3)_4$ should be considered as the multisublattice antiferromagnet. Then, detected magnetic PTs can be associated with spin reorientation of the several magnetic sublattices of this magnetic material.

It should be noted that the investigation of the behavior of elastic characteristics of magnetic materials in external magnetic field is a sensitive way of studying magnetically ordered systems.⁶ Study of the behavior of the sound velocity and absorption as function of the temperature and magnetic field allows an accurate determination of critical temperatures and fields, as well as the order of magnetic phase transitions in magnets. In the present work we have performed the study of the magnetoelastic properties of the $\text{Nd}_{0.75}\text{Dy}_{0.25}\text{Fe}_3(\text{BO}_3)_4$ single crystal in a tilted external

magnetic field. We have determined the range of angles where detected PTs^{4,5} existed and corresponding magnetic phases were stable.

2. Experimental

Isometric Nd_{0.75}Dy_{0.25}Fe₃(BO₃)₄ single crystals were grown from a fluxed solution based on bismuth trimolybdate by the procedure described in detail in Ref. 3; crystal sizes up to 10–12 mm were obtained. We worked with a crystal consisting of a transparent hexahedral prism, green in color and of the order of 5 mm high, in a direction close to an axis of symmetry of the third order (C_3). Experimental sample with characteristic dimensions $1.5 \times 1 \times 1$ mm was prepared from it. The backward x-ray reflection method (the Laue method) was used to orient the samples. The measurements of the relative changes of the velocity and attenuation of acoustic modes were performed using the automatized setup described in Ref. 7. The working frequency was 54.3 MHz. The temperature behavior of the velocity and absorption of acoustic modes (in the absence of an external magnetic field or at fixed value of the field) and the magnetic-field behavior of the same characteristics at a fixed temperature were studied. The accuracy of the relative measurements of samples with the thickness ~ 0.5 mm was about 10^{-4} in the velocity and 0.05 dB in the attenuation. The range of the temperature was 1.7–50 K, and the magnetic field up to 50 kOe was used.

3. Results

3.1. Zero magnetic field

At temperatures below 50 K we have observed three features in the behavior of the velocity of transverse and longitudinal acoustic modes: at the temperatures $T_N = 32$ K, $T_{cr2} = 25$ K, and $T_{cr1} = 16$ K. They were always accompanied by anomalies in the absorption at corresponding temperatures. Anomaly at T_N corresponds to the transition of the crystal to the magnetically ordered state, and the features at T_{cr2} and T_{cr1} are related to spin-reorientation PTs.^{4,5}

Figure 1 illustrates the typical temperature behavior of the velocity of the acoustic modes, for example of the C_{44} mode. The following notation is used in the figures: $\Delta s/s$ is the relative changes in the velocity of acoustic waves

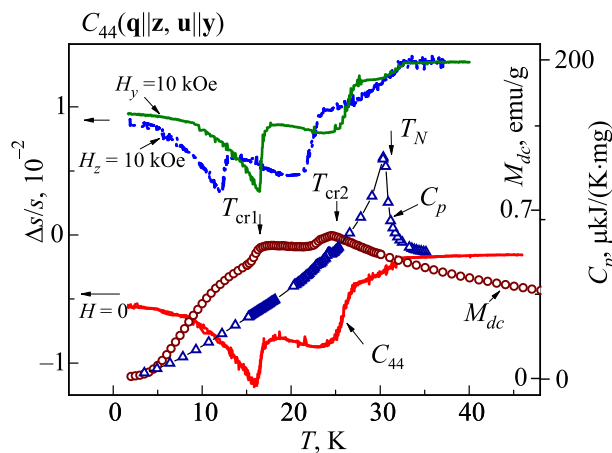


FIG. 1. Temperature dependence of the sound velocity of C_{44} acoustic mode at $H=0$ (red line), and at $H=10$ kOe [$\mathbf{H} \parallel \mathbf{z}$ (blue line); $\mathbf{H} \parallel \mathbf{y}$ (green line)] in Nd_{0.75}Dy_{0.25}Fe₃(BO₃)₄. For comparison we present the temperature behavior of the specific heat (Δ) and magnetization (\circ) (cf. Ref. 3).

(\mathbf{q} is the wave vector and \mathbf{u} is the polarization) propagating along the x , y , and z axes of the standard Cartesian coordinate system for trigonal crystals ($\mathbf{y} \parallel \mathbf{C}_2$ and $\mathbf{z} \parallel \mathbf{C}_3$). Absorption behavior was illustrated in Refs. 4 and 5, and will not be analyzed below. Figure 1 also shows the behavior of the specific heat and magnetization of the crystal in the same temperature range³ for comparison. Note that the only one anomaly at T_N is clearly observed in the behavior of the specific heat. The Néel temperature cannot be seen from the behavior of the magnetization, however, peaks at T_{cr2} and T_{cr1} are clearly visible. At the same time, the behavior of the acoustic characteristics exhibits all three critical temperatures associated with PTs in the magnetic subsystem of the crystal. This means that the coupling between magnetic and elastic subsystems is significant in this compound, which is characteristic to multiferroics. Therefore, the observation of the behavior of the elastic properties of the crystal, and their response to an external magnetic field, allows us to draw conclusions about the state of its magnetic subsystem.

3.2. The external field $\mathbf{H} \parallel \mathbf{C}_3$

The application of an external magnetic field $\mathbf{H} \parallel \mathbf{z}$ shifts the features at T_{cr2} and T_{cr1} to lower temperatures, however, the position of the feature at T_N remains virtually unchanged (cf. Fig. 1). Two closely spaced features exhibiting hysteresis were found in the magnetic field dependences of the velocity of the acoustic modes in the fields H_z^{cr1} and H_z^{cr2} (Fig. 2).

An increase of the temperature shifts them to the direction of weaker fields. Both features in the fields H^{cr1} and H^{cr2} were registered in the temperature interval from 1.7 to

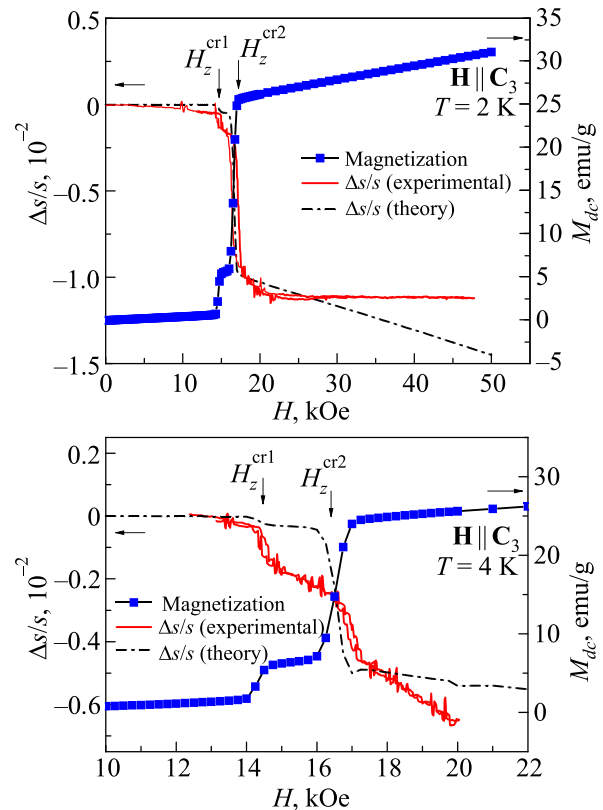


FIG. 2. Magnetic field ($\mathbf{H} \parallel \mathbf{z}$) dependence of the sound velocity (red line, the experiment; black line, calculations) of C_{44} acoustic mode and magnetization (blue symbols) in Nd_{0.75}Dy_{0.25}Fe₃(BO₃)₄ at $T=2$ (a) and $T=4$ (b) K.

16 K (T_{cr1}), while only one feature in the field H^{cr2} was detected in the range from 16 K (T_{cr1}) to 25 K (T_{cr2}). The critical fields of the features, which we observed in the behavior of the acoustic modes, and the temperature, corresponding to them, are correlated with the values of the fields and temperatures, at which magnetization anomalies were found according to the measurements performed in Ref. 3, see Fig. 2. That is why, the observed anomalies have been interpreted by us⁴ as the manifestation of magnetic reorientation PTs.

We have constructed⁴ the low-temperature fragment of the H - T phase diagram of the $\text{Nd}_{0.75}\text{Dy}_{0.25}\text{Fe}_3(\text{BO}_3)_4$ crystal for $\mathbf{H} \parallel C_3$ (z) (see Fig. 3(a)). The diagram was found to be more complex than the one presented in Ref. 2, and differs from the latter by the presence of the lines 1 and 4. Our investigations show that a few (at least three) low-temperature magnetically ordered phases exist in the compound studied in the field $\mathbf{H} \parallel z$.

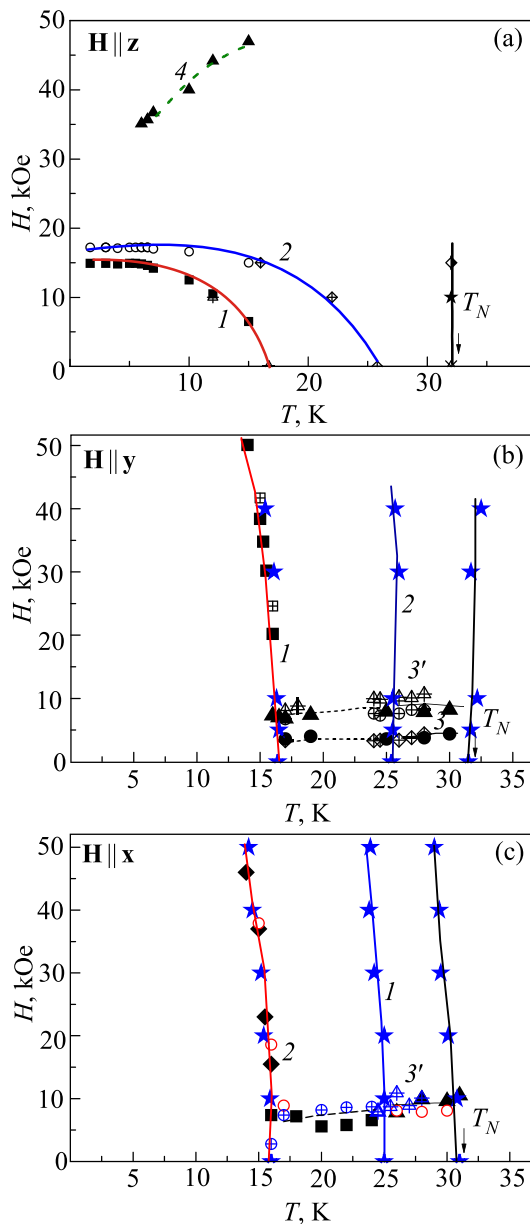


FIG. 3. External magnetic field—temperature phase diagrams for $\text{Nd}_{0.75}\text{Dy}_{0.25}\text{Fe}_3(\text{BO}_3)_4$: ($\mathbf{H} \parallel z$) (a); $\mathbf{H} \parallel y$ (b); $\mathbf{H} \parallel x$ (c). The symbols are related to the features observed in our various magnetoacoustic experiments at low temperatures and small values of the field.

3.3. The external field H applied along x and y axes

When an external magnetic field was applied in the basal plane of the crystal (both for $\mathbf{H} \parallel y$ and $\mathbf{H} \parallel x$), the features at T_{cr2} and T_{cr1} were shifted slightly toward lower temperatures. The position of the feature at T_N was essentially unchanged when the external field was applied. The example of the typical temperature behavior of sound velocity in external magnetic field $\mathbf{H} \parallel y$ is shown in Fig. 1. From the analysis of the magnetic field behavior of the acoustic modes in the external magnetic field applied in basal plane we have concluded⁵ that in the temperature range $1.7\text{ K} < T < 15\text{ K}$ the acoustic characteristics are essentially field-independent (at least for $\mathbf{H} \parallel y$). But in the temperatures range 15–32 K the behavior of the acoustic characteristics depends on the direction of the magnetic field in the basal plane. We believe that this anisotropic behavior of the acoustic characteristics observed in the $\text{Nd}_{0.75}\text{Dy}_{0.25}\text{Fe}_3(\text{BO}_3)_4$ is due to the existence of another easy axis, which is parallel to C_2 symmetry axis in the basal plane. We have observed analogous magnetic behavior in the $\text{NdFe}_3(\text{BO}_3)_4$ at the temperature range, where an easy plane, antiferromagnetic commensurate structure is realized.⁸ We have plotted the low-temperature part of the H - T phase diagrams of the crystal for fields directed along and perpendicular to the second order symmetry axis in the basal plane of the crystal (Figs. 3(b) and 3(c), respectively). To our opinion the line 3 in the H - T phase diagrams ($\mathbf{H} \parallel y$) is the line of a spin-flop transition.

3.4. Behavior in the magnetic field tilted from the crystallographic axes

Constructed phase diagrams (Fig. 3) imply the existence of several lines of PTs in the crystal in the ordered magnetic states, and, consequently, of several magnetic phases. The temperature borders (at $H = 0$) of those phases are related to three intervals:

- 1) $1.7\text{ K} < T < 16\text{ K}$ (T_{cr1});
- 2) $16\text{ K} < T < 25\text{ K}$ (T_{cr2});
- 3) $25\text{ K} < T < 32\text{ K}$ (T_N).

Let us analyze the behavior of the acoustic characteristics of the crystal in each of those intervals when the magnetic field is tilted from z axis (C_3) in the planes zy and zx , and when the field is tilted from y (C_2 axis) in the plane xy .

3.4.1. The first temperature range. Here the evolution of the magnetic field behavior of the sound velocities related to various acoustic modes with the tilt angle of the magnetic field from z axis from 0° to 90° in the zy plane at the lowest temperature of the experiment, 1.7 K, is shown in Fig. 4.

It is seen that the growth of the tilt angle up to 30° basically does not change the values of critical PT fields H_z^{cr1} and H_z^{cr2} (Fig. 4(a)). The form of anomalies (jumps) also remains the same. Further increase of the angle $\alpha > 30^\circ$ produces the shift of H_z^{cr1} and H_z^{cr2} to the higher values (Fig. 4(b)). The form of anomalies at H_z^{cr1} and H_z^{cr2} and the character of the magnetic field dependences above PT points at $\alpha > 18^\circ$ is also partly changed. Perhaps, those transitions are realized at higher values of the angle, however, their critical values of the magnetic field exceed maximal possible in our experiments value of the field 50 kOe. Hysteretic character of anomalies at H_z^{cr1} and H_z^{cr2} remains the same in the total angle range, where we registered PTs ($0 < \alpha < 65^\circ$). When $\alpha = 90^\circ$, i.e., at $\mathbf{H} \parallel y$, the sound velocity basically

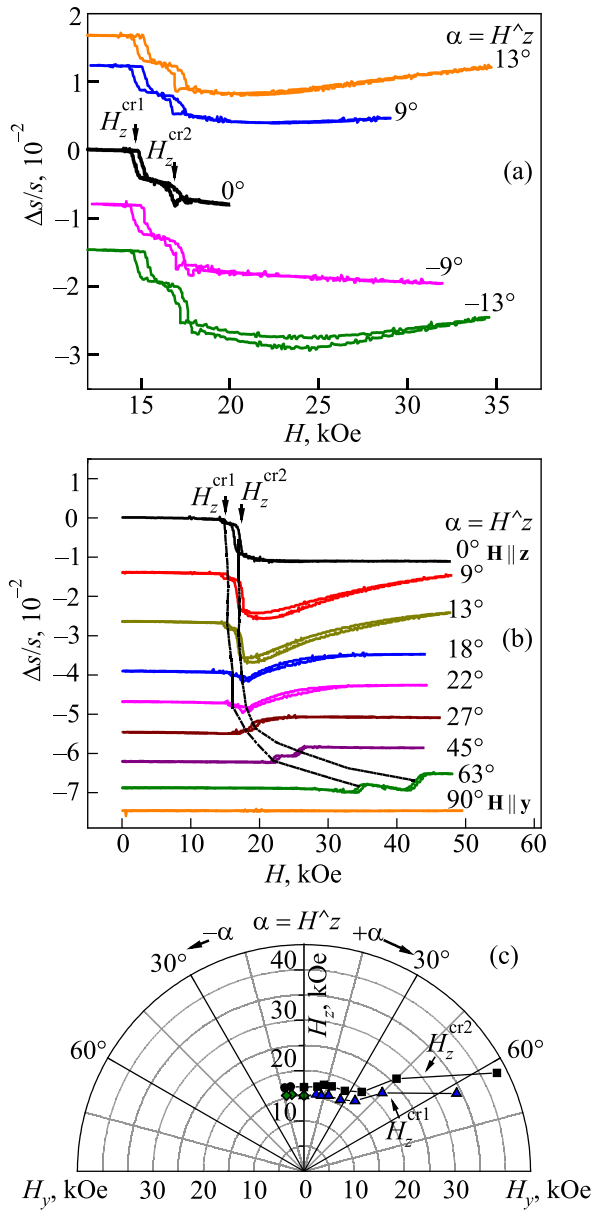


FIG. 4. Magnetic field dependencies of the sound velocity in $\text{Nd}_{0.75}\text{Dy}_{0.25}\text{Fe}_3(\text{BO}_3)_4$ at $T = 1.7\text{ K}$ for negative (a) and positive (b) values of the tilt angle from C_3 axis. Magnetic field phase diagram for $\text{Nd}_{0.75}\text{Dy}_{0.25}\text{Fe}_3(\text{BO}_3)_4$ for the magnetic field tilted from z axis in the zy plane at $T = 1.7\text{ K}$ (c).

does not depend on the value of the field (Fig. 4(b)). The dependence of H_z^{cr1} and H_z^{cr2} on the tilt angle α from the axis z (C_3) in the plane zy at 1.7 K in the polar coordinates is given in Fig. 4(c). The values H_z^{cr1} and H_z^{cr2} (in kOe) for each of the value of the tilt angle are plotted at respective radia-vectors.

In Fig. 5(b) angle dependences of H_z^{cr1} and H_z^{cr2} for two more temperature are presented: For 6 K for the tilting of the magnetic field from z axis in the zx plane (a), and for 10 K for the tilting in the zy plane. From the comparison of the angle-dependent phase diagrams (Figs. 4(c) and 5(b)) we can see that the features at H_z^{cr1} and H_z^{cr2} are registered at the tilt angles $0 \leq \alpha \leq 65^\circ$ in the zy plane, as well as in the zx plane in the first temperature interval.

However, when the tilt angle in the zx plane exceeds 30° , for all investigated temperatures in the first interval the

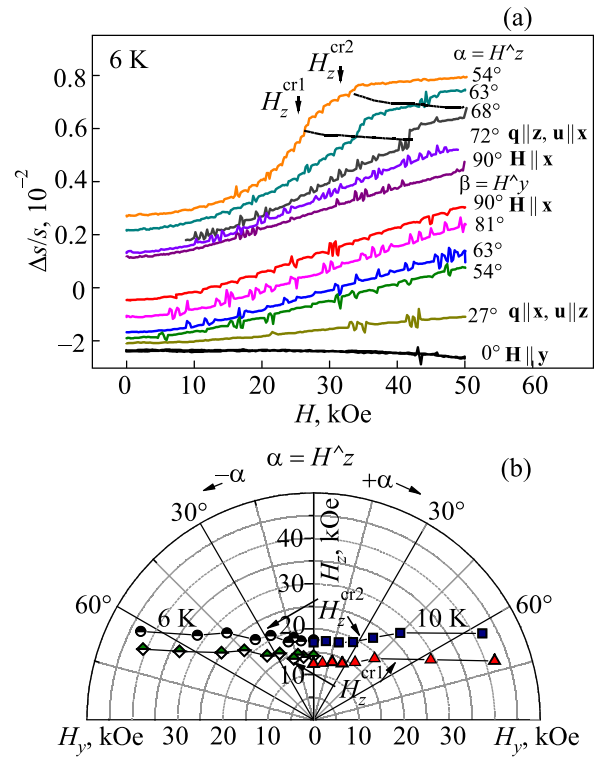


FIG. 5. Magnetic field dependencies of the sound velocity in $\text{Nd}_{0.75}\text{Dy}_{0.25}\text{Fe}_3(\text{BO}_3)_4$ at $T = 6\text{ K}$ for several values of tilt angles from C_3 axis (the angle α) and from C_2 axis (the angle β) in the zy and xy planes, respectively (a). Magnetic field phase diagram for $\text{Nd}_{0.75}\text{Dy}_{0.25}\text{Fe}_3(\text{BO}_3)_4$ for the magnetic field tilted from z axis in the zy and zx planes at $T = 6$ and 10 K (b).

smooth increase of the sound velocity is observed already in the region above the transition $H < H_z^{\text{cr1,2}}$. The anomalies themselves at H_z^{cr1} and H_z^{cr2} look like cusps, and we cannot see hysteresis. Figure 5(a) illustrates the behavior of the sound velocity related to the acoustic mode $\mathbf{q} \parallel \mathbf{x}$ and $\mathbf{u} \parallel \mathbf{z}$ at large tilt angles ($\alpha \geq 54^\circ$) in the zx plane at 6 K . With the growth of the tilt angle the features at H_z^{cr1} and H_z^{cr2} are shifted to higher values of the field. At larger tilt angles $\alpha \geq 72^\circ$ the anomalies at H_z^{cr1} and H_z^{cr2} in the applicable field range cannot be observed, however, the specifics of the monotonous increase of the sound velocity in the range below PTs keeps unchanged up to $\alpha \geq 90^\circ$, i.e., for $\mathbf{H} \parallel \mathbf{x}$.

We have also observed similar characteristic monotonous increase of the sound velocity in the case $\mathbf{H} \parallel \mathbf{x}$ for the sound mode ($\mathbf{q} \parallel \mathbf{z}$ and $\mathbf{u} \parallel \mathbf{x}$) when the field is tilted in the xy plane in the angle range $90^\circ > \beta > 20^\circ$ [here β is the tilt angle from the y axis (C_2) in the xy plane], see Fig. 5(a). For small values of the angle $0 < \beta < 20^\circ$ the sound velocity practically does not depend on the value of the magnetic field.

3.4.2. The second temperature range. The behavior of acoustic characteristics has been studied at the temperature 17 K , when the field had been tilted from the z axis in the zy and zx planes, and also in the xy plane when the field had been tilted from the y axis. At that temperature, according to the phase diagrams (Fig. 3), PTs were observed at field values $H_z^{\text{cr2}}, H_y^{\text{cr3}}, H_y^{\text{cr3}'}$, and $H_x^{\text{cr3}'}$. Let us determine the range of values of angles, where we have managed to register those phase transformations (see Figs. 6 and 7). The anomalies at the field value H_z^{cr2} , when the field is tilted in the zy and zx

planes from z axis are observed in the angle ranges $0^\circ \leq \alpha \leq 65^\circ$ and $0^\circ \leq \alpha \leq 54^\circ$, respectively. The increase of the tilt angle up to 30° in the zy and zx planes does not basically change the critical value of the field $H_z^{\text{cr}2}$. Further increase of the tilt angle in the zy plane yields the shift of $H_z^{\text{cr}2}$ to higher values.

The deviation in the plane zx for angles $\alpha \geq 30^\circ$ also shifts the anomaly in $H_z^{\text{cr}2}$ towards higher fields and yields its smearing. Monotonous growth of the sound velocity is observed in the region before transition, Fig. 6. Hence, the angle dependence of the critical field $H_z^{\text{cr}2}$ in the second range is similar to the behavior $H_z^{\text{cr}1}$ and $H_z^{\text{cr}2}$ in the first temperature range.

The features at $H_y^{\text{cr}3}$, $H_y^{\text{cr}3'}$ and $H_x^{\text{cr}3'}$ are observed when the field is tilted from the y and x axes in the xy and zx planes

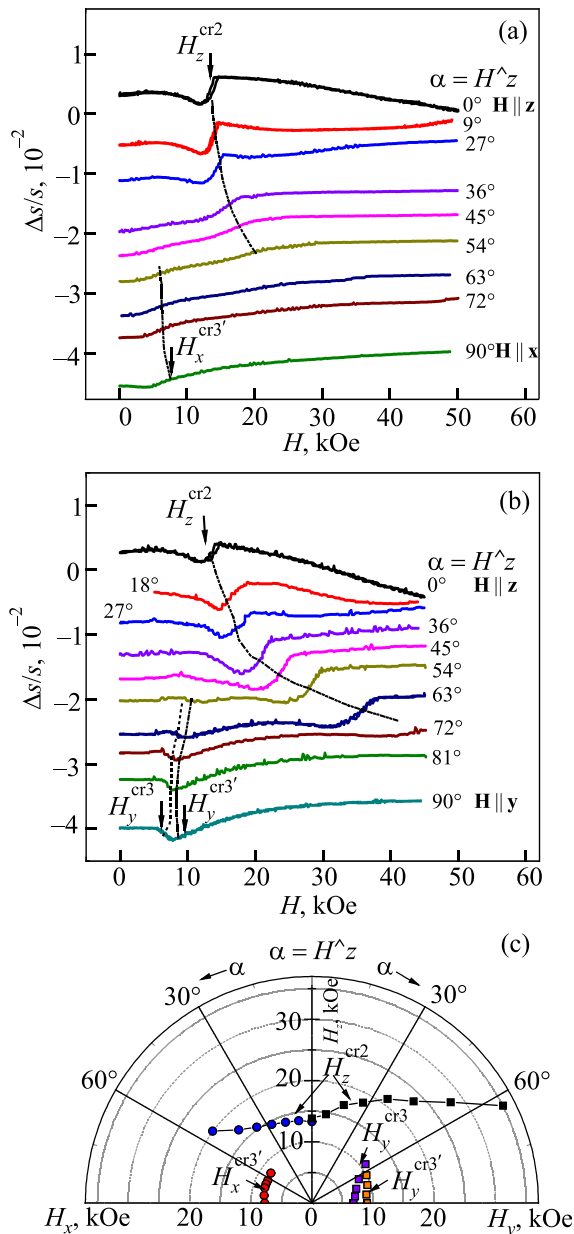


FIG. 6. Magnetic field dependencies of the sound velocity in $\text{Nd}_{0.75}\text{Dy}_{0.25}\text{Fe}_3(\text{BO}_3)_4$ at $T = 17$ K for several values of tilt angles from C_3 axis in the zx plane (a) and in the zy plane (b). Magnetic field phase diagram for $\text{Nd}_{0.75}\text{Dy}_{0.25}\text{Fe}_3(\text{BO}_3)_4$ for the magnetic field tilted from z axis in the zy and zx planes at $T = 17$ K (c).

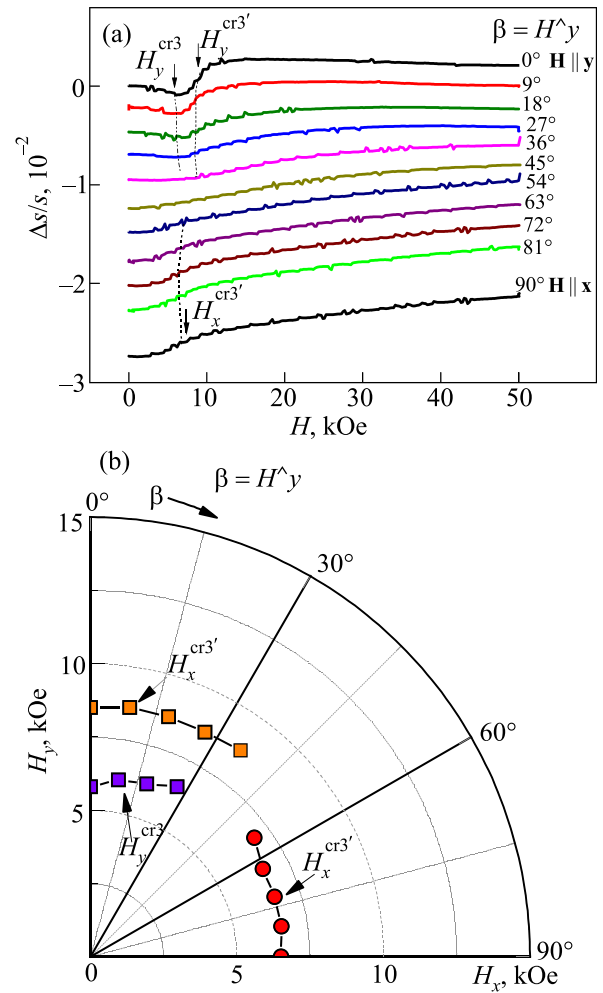


FIG. 7. Magnetic field dependencies of the sound velocity in $\text{Nd}_{0.75}\text{Dy}_{0.25}\text{Fe}_3(\text{BO}_3)_4$ at $T = 17$ K for several values of tilt angles from C_2 axis (a). Magnetic field phase diagram for $\text{Nd}_{0.75}\text{Dy}_{0.25}\text{Fe}_3(\text{BO}_3)_4$ for the magnetic field tilted from y axis in the yx plane at $T = 17$ K (b).

or angles larger than 40° , see Fig. 6. The increase of the tilt angle in the zy plane yields small shifts of $H_y^{\text{cr}3}$ and $H_y^{\text{cr}3'}$ towards larger values. The value of $H_x^{\text{cr}3'}$ is weakly dependent on the growth of the tilt angle in the zx plane. The features at $H_y^{\text{cr}3}$, $H_y^{\text{cr}3'}$ and $H_x^{\text{cr}3'}$ are observed for the deviations in the xy plane in the range of tilt angles from the y and x axes smaller than 30° .

3.4.3. The third temperature range. In that interval, according to the phase diagrams, Fig. 3, only phase transformations at $H_y^{\text{cr}3}$, $H_y^{\text{cr}3'}$ and $H_x^{\text{cr}3'}$ are realized. We have performed the investigations of angle dependences of $H_y^{\text{cr}3}$, $H_y^{\text{cr}3'}$ and $H_x^{\text{cr}3'}$ at the temperature 28 K. It turns out that at such high enough temperature (the value is close to $T_N = 32$ K) the scale of anomalies, which we attribute to phase transformations, is not large. The peculiarities themselves are smeared, and, thus, the investigation of the angle dependences of $H_y^{\text{cr}3}$, $H_y^{\text{cr}3'}$, and $H_x^{\text{cr}3'}$ has the qualitative character.

Nevertheless, the anomalies at $H_y^{\text{cr}3}$, $H_y^{\text{cr}3'}$, and $H_x^{\text{cr}3'}$ can be distinguished at tilt angles less than 45° from the y and x axes in the zy and zx planes, see Fig. 8. The values $H_y^{\text{cr}3}$, $H_y^{\text{cr}3'}$, and $H_x^{\text{cr}3'}$ become larger with the growth of tilt angles.

Magnetic field behavior of some acoustic modes, when the field is tilted in the xy plane appeared somehow unexpected. In such a geometry of the experiment we have the

opportunity to study the behavior of only those acoustic modes, that have $\mathbf{q} \parallel \mathbf{y}$ or $\mathbf{q} \parallel \mathbf{x}$.

The magnetic field dependences of the sound velocity of the transverse mode $\mathbf{q} \parallel \mathbf{y}$ and $\mathbf{u} \parallel \mathbf{z}$ for various values of tilt angle in the xy plane are presented in Fig. 9. For that mode the anomalies at $H_y^{\text{cr}3}$ and $H_y^{\text{cr}3'}$ in the field, directed exactly along y ($\mathbf{H} \parallel \mathbf{y}$) are weakly manifested. That is why, we define in the figure by arrows the values of the fields $H_y^{\text{cr}3}$ and $H_y^{\text{cr}3'}$, which are determined from the behavior of the mode $\mathbf{q} \parallel \mathbf{z}$, $\mathbf{u} \parallel \mathbf{x}$, see Fig. 8. The feature at $H_x^{\text{cr}3'}$ at $\mathbf{H} \parallel \mathbf{x}$ can be clearly seen. As one can see from the figure, the anomalies at $H_y^{\text{cr}3}$, $H_y^{\text{cr}3'}$ and $H_x^{\text{cr}3'}$ can be detected only until relatively small (less than 9°) tilt angles from the y and x axes, respectively. However, with increasing the angle (larger than 18°) in the fields $\approx H_y^{\text{cr}3}$ for $\mathbf{H} \parallel \mathbf{y}$ the new anomaly appears, which becomes more pronounced with the growth of the angle and reaches its maximum value at $\beta \approx 45^\circ$.

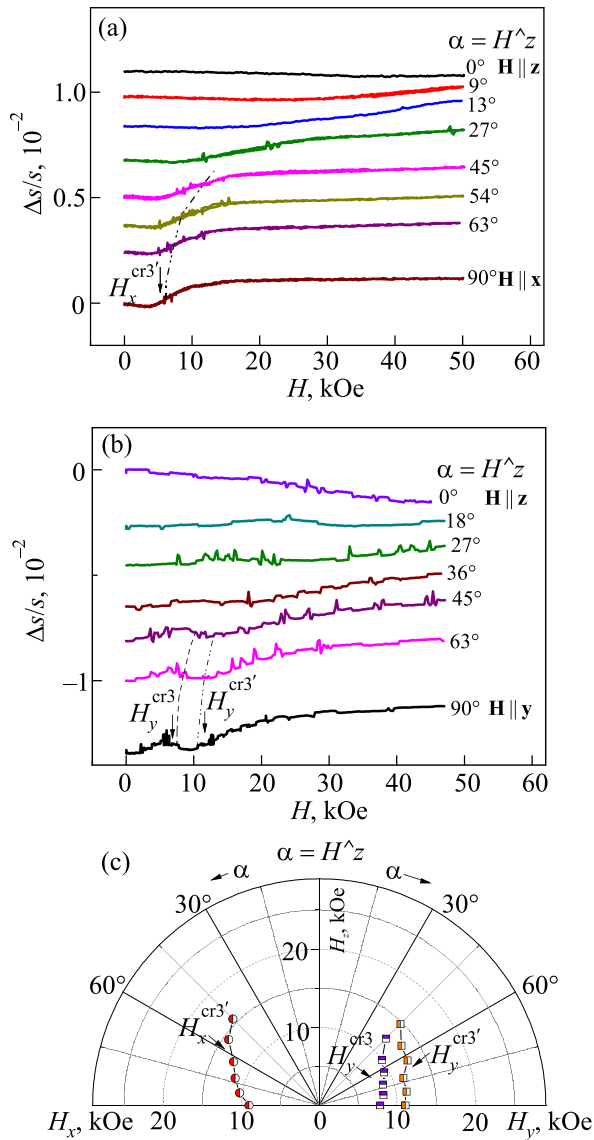


FIG. 8. Magnetic field dependencies of the sound velocity in $\text{Nd}_{0.75}\text{Dy}_{0.25}\text{Fe}_3(\text{BO}_3)_4$ at $T = 28$ K for several values of tilt angles from C_3 axis: in the zx plane (a) and in the zy plane (b). Magnetic field phase diagram for $\text{Nd}_{0.75}\text{Dy}_{0.25}\text{Fe}_3(\text{BO}_3)_4$ for the magnetic field tilted from z axis in the zy and zx planes at $T = 28$ K (c).

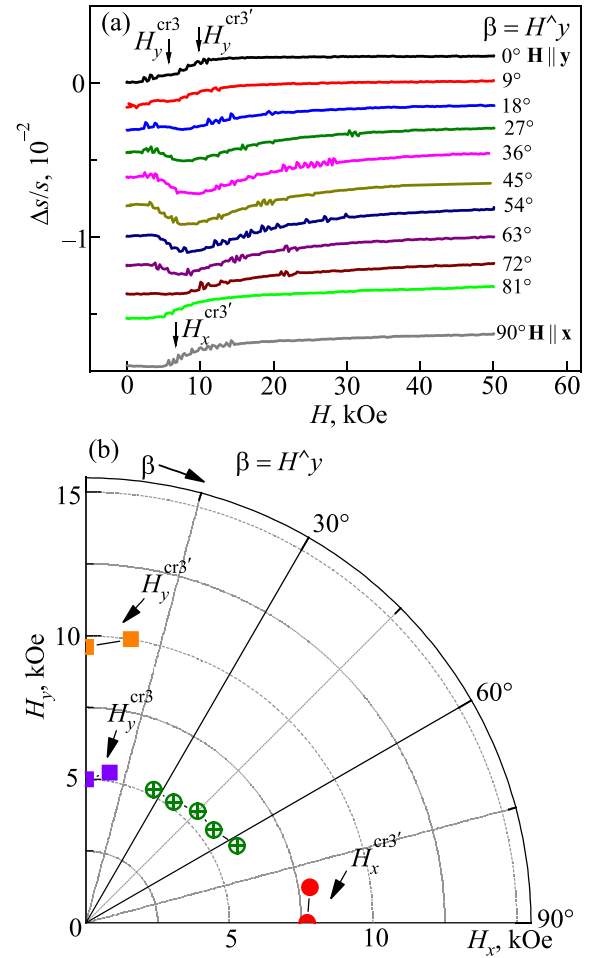


FIG. 9. Magnetic field dependencies of the sound velocity in $\text{Nd}_{0.75}\text{Dy}_{0.25}\text{Fe}_3(\text{BO}_3)_4$ at $T = 28$ K for several values of tilt angles from C_2 axis (a). Magnetic field phase diagram for $\text{Nd}_{0.75}\text{Dy}_{0.25}\text{Fe}_3(\text{BO}_3)_4$ for the magnetic field tilted from y axis in the yx plane at $T = 28$ K (b).

Hence, in the third temperature range the anomalies in the magnetic field behavior of the sound velocity (attenuation) of at least two acoustic modes are observed at any tilt angles of the magnetic field in the xy plane. Let us note that in the second range the behavior of the same modes when the field is tilted in the xy plane was different, see Fig. 7.

4. Theoretical analysis

4.1. Microscopic consideration

The following theoretical calculation was used to explain the observed experimental data. In magnetic materials the dominant contribution to the spin-lattice interactions arises mostly from the exchange-striction coupling. In our calculations we assume that in the multiferroic under study the spatial dependence of the magnetic anisotropy (i.e., of the magnetic relativistic interaction) is weaker than the spatial dependence of the exchange integrals. In this case, one can expect that mostly longitudinal sound waves interact with the spin subsystem. The magnetoacoustic interaction is considered then in the standard way in the framework of the perturbation approach.⁹ According to Refs. 9 and 10, the renormalization of the longitudinal sound velocity of such a model can be written as

$$\frac{\Delta s}{s} = -\frac{A_1 + A_2}{(N\omega_{\mathbf{q}})^2}, \quad (1)$$

where

$$\begin{aligned} A_1 &= 2|G_0^z(\mathbf{q})|^2 \langle S_0^z \rangle^2 \chi_0^z + T \sum_{\mathbf{k}} \sum_{\alpha=x,y,z} |G_{\mathbf{k}}^{\alpha}(\mathbf{q})|^2 (\chi_{\mathbf{k}}^{\alpha})^2, \\ A_2 &= H_0^z(\mathbf{q}) \langle S_0^z \rangle^2 + \frac{T}{2} \sum_{\mathbf{k}} \sum_{\alpha=x,y,z} H_{\mathbf{k}}^{\alpha}(\mathbf{q}) \chi_{\mathbf{k}}^{\alpha}. \end{aligned} \quad (2)$$

Here, N is the number of spins in the system, \mathbf{k} is the wave vector of magnetic excitations, $\omega_{\mathbf{q}} = sq$ is the low- q dispersion relation with sound velocity s in the absence of spin-phonon interactions, $\langle S_0^z \rangle$ is the average magnetization along the direction of the magnetic field, $\chi_{\mathbf{k}}^{x,y,z}$ are non-uniform magnetic susceptibilities, and the subscript 0 corresponds to $k=0$. The renormalization parameter $A_1 + A_2$ is proportional to the spin-phonon coupling constants (which have to be determined independently)

$$\begin{aligned} G_{\mathbf{k}}^{\alpha} &= \frac{1}{m} \sum_n e^{i\mathbf{k}\mathbf{R}_{nm}} (e^{i\mathbf{q}\mathbf{R}_{nm}} - 1) \mathbf{u}_{\mathbf{q}} \frac{\partial J_{mn}^{\alpha}}{\partial \mathbf{R}_m}, \\ H_{\mathbf{k}}^{\alpha} &= \frac{1}{m} \sum_n e^{-i\mathbf{k}\mathbf{R}_{nm}} (e^{i\mathbf{q}\mathbf{R}_{nm}} - 1) (e^{-i\mathbf{q}\mathbf{R}_{nm}} - 1) \\ &\quad \times \mathbf{u}_{\mathbf{q}} \mathbf{u}_{-\mathbf{q}} \frac{\partial^2 J_{mn}^{\alpha}}{\partial \mathbf{R}_n \partial \mathbf{R}_m}. \end{aligned} \quad (3)$$

Here, m is the mass of the magnetic ion, J_{mn}^{α} denote exchange integrals, $\mathbf{u}_{\mathbf{q}}$ is the polarization of the phonon with wave vector \mathbf{q} , and \mathbf{R}_n is the position vector of the n th site.^{9,10} In our calculations we used these quantities as fitting parameters. Our simplified theory reproduces the main features of the experimentally observed behavior, see Fig. 2. It

turns out that the theory reproduces the low-temperature behavior of the sound velocity rather well. On the other hand, for the higher-field region of the phase diagram the agreement is not so good. We suppose that in that phase inhomogeneous spin distribution can take place like in Nd ferroboration,⁸ resulting in nonzero inhomogeneous magnetic susceptibility, contribution of which was neglected in calculations shown in Fig. 2.

4.2. Phenomenological approach

To understand the features of the magnetic structure of the studied magnetic system of $\text{Nd}_{0.75}\text{Dy}_{0.25}\text{Fe}_3(\text{BO}_3)_4$, we have also constructed the phenomenological theory, based on the consideration of a six-sublattice antiferromagnet, cf. Refs. 4, 5, and 11. We have chosen six magnetic sublattices due to the following reasons. We have assumed that each magnetic ion (Fe, Nd, and Dy) is in the magnetically ordered state below T_N (at least in the ground state), and that each of those magnetic ions form two magnetic sublattices. Then, we have assumed that the main interaction is the exchange between iron magnetic sublattices. We also suggested that the single-ion magnetic anisotropy affects only rare earth ions, the EA anisotropy for Dy magnetic sublattices, and the EP one for the Nd sublattices, because iron ions are in the orbital singlet state. Finally, we have supposed that there exists weak interaction between iron and rare earth magnetic sublattices, and we have neglected direct interactions between rare earth sublattices. In the lowest approximation we do not take into account the weak magnetic anisotropy in the basal plane (the plane, perpendicular to C_3 axis).

The ground-state energy of such a model system in the external magnetic field H has the form

$$\begin{aligned} E &= -H[M_0 \cos(-\theta_H + \theta_1) + M_0 \cos(-\theta_H + \theta_2) + m_1 \cos(\theta_H - \varphi_1) + m_1 \cos(\theta_H - \varphi_2) + m_2 \cos(-\theta_H + \psi_1) \\ &\quad + m_2 \cos(-\theta_H + \psi_2)] + JM_0^2 \cos(\theta_1 - \theta_2) + \frac{1}{2} m_1^2 K_1 [\sin^2(\varphi_1) + \sin^2(\varphi_2)] - \frac{1}{2} m_2^2 K_2 [\sin^2(\psi_1) + \sin^2(\psi_2)] \\ &\quad + J_1 M_0 m_1 [\cos(\theta_1 - \varphi_1) + \cos(\theta_1 - \varphi_2) + \cos(\theta_2 - \varphi_1) + \cos(\theta_2 - \varphi_2)] \\ &\quad + J_2 M_0 m_2 [\cos(-\theta_1 + \psi_1) + \cos(-\theta_1 + \psi_2) + \cos(-\theta_2 + \psi_1) + \cos(-\theta_2 + \psi_2)]. \end{aligned} \quad (4)$$

Here we denote by M_0 the magnitude of the iron magnetic sublattice with $\theta_{1,2}$ being the angles between two iron sublattices and C_3 axis, by $m_{1,2}$ the magnitudes of rare earth magnetic sublattices of Nd and Dy ions, respectively (with $\varphi_{1,2}$ and $\psi_{1,2}$ being angles between Nd and Dy magnetic sublattices, respectively, and the C_3 axis), θ_H denotes the angle between the direction of the external magnetic field and C_3 axis, $J > 0$ defines the iron-iron antiferromagnetic exchange interaction, $K_{1,2} > 0$ are the EP and EA magnetic anisotropies for Nd and Dy magnetic sublattices, respectively, and, finally, $J_{1,2}$ are the couplings between iron and rare earth magnetic sublattices.

To determine the steady-state magnetic configurations of the considered model we minimize the expression for the

ground-state energy with respect to the angles $\theta_{1,2}$, $\varphi_{1,2}$, and $\psi_{1,2}$. The analysis is very complicated. For example, even for $\theta_H = 0$, i.e., for the external magnetic field directed along C_3 axis, we have found 27 solutions of the minimization conditions. They correspond to the anti-parallel, parallel and tilted configurations of each pair of magnetic sublattices.

Let us consider those solutions. The phase with each of three pairs of sublattices being antiparallel (the antiferromagnetic solution) is related to the case with $\theta_2 = \varphi_2 = \psi_2 = \pi$ and $\theta_1 = \varphi_1 = \psi_1 = 0$ (or vice versa). Such an antiferromagnetic state has the energy $E_{AF} = -JM_0^2$. Obviously, that phase has the minimal energy in the absence of the external magnetic field.

There are three solutions with two pairs of magnetic sublattices being antiparallel, and one pair of sublattices in the tilted (spin-flop-like) state. The first such phase has $\varphi_2 = \psi_2 = \pi$, $\varphi_1 = \psi_1 = 0$, and $\theta_2 = -\theta_1$ with

$$\cos \theta_1 = \frac{H}{2JM_0}. \quad (5)$$

It has the energy $E_{2AF2} = (M_0H/2) - (H^2/J)$. The second solution has the values of angles $\theta_2 = \psi_2 = \pi$, $\theta_1 = \psi_1 = 0$ and $\varphi_2 = -\varphi_1$ with

$$\cos \varphi_1 = \frac{H}{m_1K_1}. \quad (6)$$

It has the energy $E_{2AF4} = (H^2/K_1) - JM_0^2 + m_1^2K_1$. Finally, the third such solution is related to the values of angles $\theta_2 = \varphi_2 = \pi$, $\theta_1 = \varphi_1 = 0$ and $\psi_2 = -\psi_1$ with

$$\cos \psi_1 = \frac{H}{m_2K_2}. \quad (7)$$

This phase has the energy $E_{2AF6} = -(H^2/K_2) - JM_0^2 - m_2^2K_2$.

There are three solutions with two pairs of magnetic sublattices being antiparallel, and one pair of sublattices being parallel (and directed along the field). The first such solution has $\varphi_2 = \psi_2 = \pi$, $\varphi_1 = \psi_1 = 0$ and $\theta_2 = -\theta_1$ with $\theta_1 = 0$. It has the energy $E_{2AF1} = -2HM_0 + JM_0^2$. The second one has the values of angles $\theta_2 = \psi_2 = \pi$, $\theta_1 = \psi_1 = 0$, and $\varphi_2 = -\varphi_1$ with $\varphi_1 = 0$. It has the energy $E_{2AF3} = -2Hm_1 - JM_0^2$. The third such solution is related to the values of angles $\theta_2 = \varphi_2 = \pi$, $\theta_1 = \varphi_1 = 0$ and $\psi_2 = -\psi_1$ with $\psi_1 = 0$. This solution has the energy $E_{2AF5} = -2Hm_2 - JM_0^2$. Possible field-governed PTs between these three phases and three previous phases are of the second order.

There are 12 phases in which only one pair of sublattices is antiparallel.

Among them there are three solutions with one pair of sublattices being antiparallel, and two others being in the spin-flop-like (tilted) state. The first one of those phases has $\psi_2 = \pi$, $\psi_1 = 0$ with $\theta_2 = -\theta_1$, $\varphi_2 = -\varphi_1$ and with

$$\begin{aligned} \cos \theta_1 &= \frac{H(K_1 + 2J_1)}{2M_0(K_1J + 2J_1^2)}, \\ \cos \varphi_1 &= \frac{H(J_1 - J)}{m_1(K_1J + 2J_1^2)}. \end{aligned} \quad (8)$$

This state has the energy

$$\begin{aligned} E_{AF4} &= (2m_1^2K_1^3J^2 + J^2M_0HK_1^2 + 2J^2K_1M_0HJ_1 \\ &+ 2H^2K_1J^2 - 2H^2K_1^2J + 8m_1^2K_1^2JJ_1^2 + 2JK_1M_0HJ_1^2 \\ &- 8H^2J_1K_1J + 4JM_0HJ_1^3 + 8m_1^2K_1J_1^4 \\ &- 2H^2K_1J_1^2 - 8H^2J_1^3)/2(K_1J + 2J_1^2)^2. \end{aligned}$$

The second one is related to the following set of angles $\varphi_2 = \pi$, $\varphi_1 = 0$ with $\theta_2 = -\theta_1$, $\psi_2 = -\psi_1$ and

$$\begin{aligned} \cos \theta_1 &= \frac{H(2J_2 - K_2)}{2M_0(-K_2J + 2J_2^2)}, \\ \cos \psi_1 &= \frac{H(J_2 - J)}{m_2(-K_2J + 2J_2^2)}. \end{aligned} \quad (9)$$

It has the energy

$$\begin{aligned} E_{AF8} &= -(2m_2^2K_2^3J^2 - J^2M_0HK_2^2 + 2J^2K_2M_0HJ_2 \\ &+ 2H^2K_2J^2 + 2H^2K_2^2J - 8m_2^2K_2^2JJ_2^2 - 8H^2J_2K_2J \\ &+ 2JK_2M_0HJ_2^2 - 4JM_0HJ_2^3 + 8m_2^2K_2J_2^4 - 2H^2K_2J_2^2 \\ &+ 8H^2J_2^3)/2(K_2J - 2J_2^2)^2. \end{aligned}$$

Finally, the third one corresponds to the set of angles $\theta_2 = \pi$, $\theta_1 = 0$, $\varphi_2 = -\varphi_1$, $\psi_2 = -\psi_1$ with

$$\cos \varphi_1 = -\frac{H}{m_1K_1}, \quad \cos \psi_1 = \frac{H}{m_2K_2}. \quad (10)$$

The energy of such a state is equal to

$$\begin{aligned} E_{AF12} &= (H^2K_2 - H^2K_1 - JM_0^2K_1K_2 \\ &+ m_1^2K_1^2K_2 - m_2^2K_2^2K_1)/K_1K_2. \end{aligned}$$

Six such solutions have one pair of sublattices antiparallel, one pair parallel (and directed along the field), and one pair in the tilted state. The angles, corresponding to antiparallel state are either zero or π , the angles related to the parallel state are zero, and the angles for sublattices in the tilted states differ from each other by their signs. The solutions are

$$\cos \theta_1 = \frac{H - 2J_1m_1}{2JM_0}, \quad (11)$$

with the energy

$$\begin{aligned} E_{AF2} &= -(2H^2 - 8HJ_1m_1 + 4Hm_1J - JM_0H \\ &+ 2Jm_0J_1m_1 + 8J_1^2m_1^2)/2J; \\ \cos \theta_1 &= \frac{H}{2JM_0}, \end{aligned} \quad (12)$$

with $E_{AF6} = -H(2H + 4m_2J - JM_0 - 4J_2m_2)/2J$;

$$\cos \varphi_1 = \frac{2J_1M_0 - H}{m_1K_1}, \quad (13)$$

with the energy

$$\begin{aligned} E_{AF3} &= (-2HM_0K_1 - 4HJ_1M_0 + H^2 \\ &+ JM_0^2K_1 + 4J_1^2M_0^2 + m_1^2K_1^2)/K_1; \\ \cos \varphi_1 &= \frac{-H}{m_1K_1}, \end{aligned} \quad (14)$$

with the energy

$$\begin{aligned} E_{AF11} &= (H^2 - 2Hm_2K_1 - JM_0^2K_1 + m_1^2K_1^2)/K_1; \\ \cos \psi_1 &= \frac{H}{m_2K_2}, \end{aligned} \quad (15)$$

with the energy

$$\begin{aligned} E_{AF7} &= -(2HM_0K_2 + H^2 - JM_0^2K_2 \\ &- 4J_2M_0H + m_2K_2^2)/K_2; \end{aligned}$$

and

$$\cos \psi_1 = \frac{H}{m_2K_2}, \quad (16)$$

with the energy

$$E_{AF10} = -(2Hm_1K_2 + H^2 + JM_0^2K_2 + m_2^2K_2^2)/K_2.$$

There are three solutions with one pair of sublattices being antiparallel, and two other pairs being parallel and directed along the magnetic field. The angles for antiparallel states are equal to zero and π , and the angles in parallel states are equal to zero. The energies of those phases are

$$\begin{aligned} E_{AF1} &= -H(2M_0 + 2m_1) + JM_0^2 + 4J_1M_0m_1, \\ E_{AF5} &= -H(2M_0 + 2m_2) + JM_0^2 + 4J_2M_0m_2, \\ E_{AF9} &= -H(2m_1 + 2m_2) - JM_0^2. \end{aligned}$$

Then there exists a solution with all three pairs of sublattices being in the tilted phases. For that phase we get different signs for angles belonging to opposite sublattices with

$$\begin{aligned} \cos \theta_1 &= \frac{H(2J_2K_1 + 2J_1K_2 - K_1K_2)}{2M_0(2J_2^2K_1 - 2J_1^2K_2 - JK_1K_2)}, \\ \cos \varphi_1 &= \frac{H(JK_2 - J_1K_2 + 2J_1J_2 - 2J_2^2)}{m_1(2J_2^2K_1 - 2J_1^2K_2 - JK_1K_2)}, \\ \cos \psi_1 &= \frac{H(-JK_1 + J_2K_1 + 2J_1J_2 - 2J_1^2)}{m_2(2J_2^2K_1 - 2J_1^2K_2 - JK_1K_2)}, \end{aligned} \quad (17)$$

with the energy

$$\begin{aligned} E_{3F} &= -(8m_2^2K_2^2J_2^2K_1^2J + 8m_2^2K_2^3J_1^2JK_1 - 8m_1^2K_1^2J_1^2K_2^2J - 16m_2^2K_2^2J_2^2K_1J_1^2 - 8m_1^2K_1^3J_1^4 + 8H^2J_2^2J_1^2K_2 \\ &+ 2H^2J^2K_1^2K_2 - 8H^2J_1^2J_2^2K_1 - 2H^2K_2K_1^2J_2^2 + 2H^2K_2^2K_1J_2^2 - 16H^2JK_2^2J_1^2 - 2H^2J^2K_2^2K_1 + 16H^2J_1J_2^3K_1 \\ &- 16H^2J^3J_2K_2 + 16m_1^2K_1^2J_2^2J_1^2K_2 + 8m_1^2K_1^3J_2^2JK_2 + 8H^2J_2^3K_1^2 - 8H^2J_2^4K_1 + 8H^2J_1^4K_2 + 8J_1^3H^2K_2^2 \\ &+ 8m_2^2K_2J_2^2K_1^2 + 2m_2^2K_2^3J_2^2K_1^2 - 8m_1^2K_1J_1^4K_2^2 - 2m_1^2K_1^3J_2^2K_2^2 - 8H^2J_2K_1^2JK_2 + 8H^2JK_2J_2^2K_1 \\ &+ 8H^2JK_1J_1^2K_2 - 8J_1H^2K_2K_1J_2^2 - 8H^2J_2K_1J_1^2K_2 - HJ^2K_1^2K_2^2M_0 + 4HJJ_1^3K_2^2M_0 - 4HJJ_2^3K_1^2M_0 \\ &+ 2HJ^2J_1K_1K_2^2M_0 + 2HJ^2J_2K_1^2K_2M_0 - 2HJJ_1^2K_1K_2^2M_0 + 2HJJ_2^2K_1^2K_2M_0 \\ &+ 4HJ_1^2J_2JK_1K_2M_0 - 4HJJ_1J_2^2K_1K_2M_0)/2(JK_1K_2 - 2J_2^2K_1 + 2J_1^2K_2)^2. \end{aligned}$$

There are three solutions with two pairs of sublattices being in the tilted phases and one pair being parallel and directed along the field. The angles for parallel states are zero, and the ones for tilted states have different signs. The first such a state has the angles

$$\cos \theta_1 = \frac{H(K_2 - 2J_2) - 2J_1m_1K_2}{2M_0(J_1K_2 - J_2^2)}, \quad \cos \psi_1 = \frac{H(2J_1 - 2J_2) + 4J_1J_2m_1}{2m_2(J_1K_2 - J_2^2)}, \quad (18)$$

with the energy

$$\begin{aligned} E_{F1} &= (8J_1^2K_2HM_0J_2m_1 + 2J_1K_2JM_0^2HJ_2 - 2J_1K_2JM_0^2m_1J_2^2 + 16J_1K_2HM_0m_1J_2^2 - 8M_0^2HJ_2^4 + 8M_0H^2J_2^3 \\ &+ 4H^2J_2^3m_1 + K_2JM_0^2HJ_2^2 - 8J_1^2K_2^2HM_0m_1 + 2J_1^2K_2JM_0^2m_1 - 16J_1^2K_2^2M_0m_1^2J_2^2 - 8J_1^2K_2M_0^2HJ_2 - 16J_1^2K_2J_2^2M_0^2m_1 \\ &- 4J_1K_2^2m_2^2M_0J_2^2 - J_1K_2^2JM_0^2H + 8J_1K_2J_2^2M_0^2H - 4J_1K_2M_0H^2J_2 - 4J_1K_2H^2J_2m_1 + 4J_1K_2Hm_1^2J_2^2 - 16J_1HM_0J_2^3m_1 \\ &- 2JM_0^2HJ_2^3 - 2K_2H^2m_1J_2^2 + 2K_2m_2^2M_0J_2^4 + 8M_0m_1^2K_2^2J_1^3 + 2J_1^2m_2^2M_0K_2^3 - 4J_1^2K_2^2m_1^2H + 2J_1^2M_0H^2K_2 \\ &+ 2J_1M_0H^2K_2^2 + 2J_1K_2^2m_1H^2 + 16J_1J_2^4M_0^2m_1 + 8J_1J_2^3M_0^2H - 4J_1M_0H^2J_2^2 - 4M_0H^2K_2J_2^2)/2M_0(J_1K_2 - J_2^2)^2. \end{aligned}$$

The second one has angles

$$\cos \theta_1 = \frac{H(K_1 + 2J_1) - 2J_2m_2K_1}{2M_0(J_2K_1 + J_1^2)}, \quad \cos \varphi_1 = -\frac{H(K_1 + 2J_1) - 2J_2m_2K_1}{2M_0(J_2K_1 + J_1^2)}, \quad (19)$$

with the energy

$$\begin{aligned} E_{F2} &= -(-2m_1^2K_1J_1^4 + 4Hm_2J_1^4 - 2JM_0HJ_1^3 + 2J_1^2M_0J_2m_2K_1 + 4H^2J_2J_1^2 - 4m_1^2K_1^2J_2J_1^2 - J_1^2JM_0HK_1 \\ &+ 8Hm_2J_1^2J_2K_1 + 8H^2J_1J_2K_1 - 16HJ_1J_2^2m_2K_1 - 2J_1JM_0J_2K_1H + 2H^2K_1^2J_2 + 8J_2^3m_2^2K_1^2 + 2JM_0J_2^2K_1^2m_2 \\ &- JM_0J_2K_1^2H - 2m_1^2K_1^3J_2^2 - 2H^2J_2^2K_1 - 4J_2^2m_2HK_1^2)/2(J_2K_1 + J_1^2)^2. \end{aligned}$$

The third such state has the values of the angles

$$\cos \varphi_1 = \frac{2J_1M_0 - H}{m_1K_1}, \quad \cos \psi_1 = \frac{H - 2J_2M_0}{m_2K_2}, \quad (20)$$

with the energy

$$E_{F3} = -(2HM_0K_1K_2 + 4HK_2J_1M_0 - K_2H^2 - 4HK_1J_2M_0 + K_1H^2 - JM_0^2K_1K_2 - m_1^2K_1^2K_2 - 4K_2J_1^2M_0^2 + m_2^2K_2^2K_1 + 4K_1J_2^2M_0^2)/K_1K_2.$$

There are three solutions with one pair of sublattices being in the tilted phase, and two other pairs being parallel (and directed along the field). The states with parallel sublattices have angles equal to zero, and those in the tilted states have opposite signs of angles for the pair of sublattices with

$$\cos \theta_1 = -\frac{H - 2J_1m_1 - 2J_2m_2}{2JM_0} \quad (21)$$

with the energy

$$E_{2F3} = (2H^2 - 8HJ_1m_1 - 8HJ_2m_2 + 4Hm_1J + 4Hm_2J - JM_0H + 2JM_0J_1m_1 + 2JM_0J_2m_2 + 8J_1^2m_1^2 + 16J_1m_1J_2m_2 + 8J_2^2m_2^2)/2J;$$

with

$$\cos \varphi_1 = \frac{-H + 2J_1M_0}{m_1K_1}, \quad (22)$$

and the energy

$$E_{2F2} = (-2HM_0K_1 + H^2 - 4HJ_1M_0 - 2Hm_2K_1 + JM_0^2K_1 + 4J_1^2M_0^2 + 4J_2M_0m_2K_1 + m_1^2K_1^2)/K_1;$$

and with

$$\cos \psi_1 = \frac{H - 2J_2M_0}{m_2K_2}, \quad (23)$$

with the energy

$$E_{2F1} = -(2HM_0K_2 + 2Hm_1K_2 + H^2 - 4HJ_2M_0 - JM_0^2K_2 - 4J_1M_0m_1K_2 + 4J_2^2M_0^2 + m_2^2K_2^2)/K_2.$$

Finally, there exists a ferromagnetic solution, where all sublattices are parallel and directed along the field, i.e., $\theta_1 = \theta_2 = \varphi_1 = \varphi_2 = \psi_1 = \psi_2 = 0$ with the energy

$$E_F = -2H(M_0 + m_1 + m_2) + JM_0^2 + 4J_1M_0m_1 + 4J_2M_0m_2.$$

Obviously, this ferromagnetic state is realized at large values of the external magnetic field.

When the value of the external magnetic field grows, one should, generally speaking, observe all possible field-induced transitions between the above presented solutions. As a rule, the transitions between antiparallel and tilted state of the same pair of sublattices are first order transitions (spin-flop-like), while the transitions between the tilted and parallel directions of sublattices are of the second order.

We have also obtained analytical solutions for $\theta_H = \pi/2$, i.e., the external magnetic field is directed in the basal xy plane, perpendicular to C_3 . Notice that this case cannot be

applied to the considered system directly, because of the in-plane magnetic anisotropy in $\text{Nd}_{0.75}\text{Dy}_{0.25}\text{Fe}_3(\text{BO}_3)_4$. In that case the symmetry implies $\theta_2 = \pi - \theta_1$; $\varphi_2 = \pi - \varphi_1$ and $\psi_2 = \pi - \psi_1$. There are several solutions, which can be realized.

In the case $H = 0$, we have $\theta_1 = \varphi_1 = \psi_1 = 0$. For weak nonzero H the tilt angles are

$$\begin{aligned} \sin \theta_1 &= \frac{H(-K_1K_2 + 2J_2K_1 - 2J_1K_2)}{M_0(JK_1K_2 + 4J_2^2K_1 - 4J_1^2K_2)}, \\ \sin \varphi_1 &= \frac{H(-JK_2 + 4J_1J_2 - 4J_2^2 - 2J_1K_2)}{m_1(JK_1K_2 + 4J_2^2K_1 - 4J_1^2K_2)}, \\ \sin \psi_1 &= \frac{H(JK_1 + 4J_1J_2 - 4J_1^2 + 2J_2K_1)}{m_2(JK_1K_2 + 4J_2^2K_1 - 4J_1^2K_2)}. \end{aligned} \quad (24)$$

When the value of the external field becomes larger pairs of magnetic sublattices become parallel to the direction of the field, step by step. First, the one pair of rare earth sublattices become field-directed, e.g., Nd one with $\cos \varphi_1 = 0$, and with

$$\begin{aligned} \sin \theta_1 &= \frac{-HK_2 + 2J_1m_1K_2 + 2HJ_2}{M_0(JK_2 + 4J_2^2)}, \\ \sin \psi_1 &= \frac{JH + 2J_2H - 4J_1J_2m_1}{m_2(JK_2 + 4J_2^2)}, \end{aligned} \quad (25)$$

at

$$H = \frac{m_1(JK_1K_2 + 4J_2^2K_1 - 4J_1^2K_2)}{-JK_2 + 4J_1J_2 - 4J_2^2 - 2J_1K_2}.$$

(or, vice versa, the angle ψ_1 , for Dy sublattices becomes $\pi/2$ with the angle φ_1 for Nd sublattices being tilted, depending on the relative values of $J_{1,2}$ and $K_{1,2}$).

Then two pairs of rare earth sublattices become parallel to the direction of the field, $\cos \varphi_1 = \cos \psi_1 = 0$, in the considered case at

$$H = [m_2(JK_2 + 4J_2^2) + 4J_1J_2m_1]/(J + 2J_2).$$

Here the tilt angle for iron sublattices is

$$\sin \theta_1 = \frac{-H + 2J_1m_1 + 2J_2m_2}{JM_0}. \quad (26)$$

Finally, at the largest value of the field, in the considered case at $H = JM_0 - 2J_1m_1 - 2J_2m_2$, all magnetic sublattices become parallel to the direction of the external field.

The PTs for $\mathbf{H} \perp C_3$ are of the second order for the considered model.

The analysis can be significantly simplified when we take into account that $J \gg K_{1,2} \gg J_{1,2}$. In this case the tilted states for the field directed along C_3 for Nd sublattices have angles

$$\cos \varphi_1 \approx -\frac{H}{m_1K_1}, \quad (27)$$

for Dy sublattices the angles are

$$\cos \psi_1 \approx \frac{H}{m_2K_2}, \quad (28)$$

and for the iron sublattices the tilt angle is

$$\cos \theta_1 \approx \frac{H}{2JM_0}. \quad (29)$$

Then the main PTs occur between the states with antiparallel directions of rare earth sublattices to the tilted ones (with the iron sublattices being in the antiparallel state), following by transition in the iron sublattice subsystem from the antiparallel to the tilted state. These PTs between the antiparallel states of sublattices to the tilted ones are of the first order (of the spin-flop type). Then at much higher values of the field, directed along z , first rare earth sublattices flip to the ferromagnetic state along the field direction (at the field values $H = |m_1K_1|$ and $H = m_2K_2$), and, finally, iron sublattices flip to the ferromagnetic state at $H = 2JM_0$. From the estimates of the critical values of the field, connected to our experiments, we can assume that we observe field-induced first order transitions, related to the former case of the field, directed along C_3 , while we do not have enough field strength to observe the PTs to the latter case of the transitions to the parallel sublattices.

We suppose that in the real system the values of critical fields are very close to each other, and, hence, it is difficult to distinguish all such PTs, especially at the conditions of the experiment $T \neq 0$ (at least in the second and third temperature ranges).

On the other hand, in this approximation for $\theta_H = \pi/2$ (field, directed in the basal xy plane), the tilt angles become

$$\sin \theta_1 \approx -\frac{H}{M_0J}, \quad \sin \varphi_1 \approx -\frac{H}{m_1K_1}, \quad \sin \psi_1 \approx \frac{H}{m_2K_2}. \quad (30)$$

When the field value grows the first rare earth magnetic sublattices flip to the state, parallel to the direction of the field at $H = |m_1K_1|$ and $H = m_2K_2$, and, finally, the iron magnetic sublattices become parallel to the field direction at $H = |M_0J|$. Those PTs are of the second order. In our experiments we observe first order transitions related to the value of the in-plane magnetic anisotropy. This case cannot be studied analytically yet.

The theoretical analysis of the direction of the external magnetic field tilted from C_3 and tilted from C_2 in the basal plane is very complicated and have not yet permitted us to obtain analytical results. Even for two magnetic sublattices such an analysis can be realized analytically only for small values of the tilt angles.^{12,13} Our study for the considered six-sublattice model of the antiferromagnet implies that the critical values of tilt angles, at which the first order phase transitions transform to the second order ones¹² are larger than for the two-sublattice antiferromagnetic model. On the one hand, this is related to the considered approximation (singlet orbital state of the iron sublattices, and the absence of the direct interaction between rare earth sublattices themselves), and, on the other hand, it qualitatively agrees with our experimental findings in $\text{Nd}_{0.75}\text{Dy}_{0.25}\text{Fe}_3(\text{BO}_3)_4$.

We can take into account nonzero temperatures, using the method developed in Ref. 14. The results of Ref. 14 imply that the values of the critical fields depend on T as $H^c = H^c(T=0)a(T)$, where $a(T)$ is the component of the

order parameter, characteristic for the considered magnetic phase, which decreases with the growth of T from the maximal value at $T=0$ to zero at $T=T_c$. Such a consideration qualitatively describes the features of the obtained phase H - T diagrams in $\text{Nd}_{0.75}\text{Dy}_{0.25}\text{Fe}_3(\text{BO}_3)_4$.

5. Summary

In summary, we have performed low-temperature magnetoacoustic investigations of rare earth ferrobortate $\text{Nd}_{0.75}\text{Dy}_{0.25}\text{Fe}_3(\text{BO}_3)_4$. We have observed how the features of the sound velocity behavior in the magnetic field were changed due to the tilting of the direction of the external magnetic field from the main crystallographic axes C_3 and C_2 in all observed temperature regions, where magnetic orderings exist. Our observations show that magnetic phase transitions exist for large enough values of the tilting of the external magnetic field from C_3 axis. In the lowest temperature range the behavior for tilting in the zy and zx planes is similar. In the intermediate temperature phase, on the other hand, the behavior of the magnetic field-induced phase transitions were different for deviations of the field direction from C_3 in the zy and zx planes. Also in this temperature range we registered field-governed phase transitions when the field is tilted from the crystallographic axes in the xy (basal) plane. The latter can be seen also, when we tilt the direction of the external magnetic field from the basal plane towards C_3 axis. In the highest-temperature ordered phase we observed phase transition for the field tilted from the basal plane towards z , with the similar field behavior, comparing with the intermediate phase. Contrary, the features for the tilting of the field from C_2 axis are manifested much weaker than those in the intermediate temperature phase.

We have also performed comparison of our experimental findings with the results of the developed microscopic and phenomenological theories. Our theory agrees with our earlier assumption^{4,5} about multisublattice nature of the magnetically ordered phases in the considered ferrobortate. According to the phenomenological consideration, there can exist many field-induced magnetic phases in the system, the transitions between some of them being very close to each other. We can observe only few of them in the experimentally available magnetic field and temperature intervals. Our analysis permits us to assume that for higher field region inhomogeneous magnetic state can take place for the magnetic field directed along C_3 . Our phenomenological analysis qualitatively agrees with the mean field approach developed in Ref. 11 and with our experimental findings. We can suppose that the large values of the field and tilt angle values, at which the first order phase transitions transform to the second order ones, comparing to the standard two-sublattice antiferromagnet, are related to the features of the studied rare earth ferrobortates. Namely, we think that it is related, first, to the singlet state of iron ions (which, from this viewpoint, have to be more magnetically isotropic, while the magnetic anisotropy is caused mostly by the rare earth magnetic ions). Second, it is connected with the relatively weak coupling between rare earth magnetic ions with iron ones, and with the almost absent interaction between rare earth magnetic ions themselves.

The study was supported by Grant of the Russian Federation president on support of sciences schools No.

4828.2012.2, and The Ministry of education and science of Russian Federation, Project No. 8365.

^{a)}Email: zvyagina@ilt.kharkov.ua

¹A. M. Kadomtseva, Yu. F. Popov, G. P. Vorob'ev, A. P. Pyatakov, S. S. Krotov, P. I. Kamilov, V. Yu. Ivanov, A. A. Mukhin, A. K. Zvezdin, L. N. Bezmaternykh, I. A. Gudim, and V. L. Temerov, *Fiz. Nizk. Temp.* **36**, 640 (2010) [[Low Temp. Phys.](#) **36**, 511 (2010)].

²Yu. F. Popov, A. M. Kadomtseva, G. P. Vorob'ev, A. A. Mukhin, V. Yu. Ivanov, A. M. Kuz'menko, A. S. Prokhorov, L. N. Bezmaternykh, and V. L. Temerov, *Pis'ma Zh. Eksp. Teor. Fiz.* **89**, 405 (2009).

³I. A. Gudim, E. V. Eremin, and V. L. Temerov, *J. Cryst. Growth* **312**, 2427 (2010).

⁴G. A. Zvyagina, K. R. Zhekov, A. A. Zvyagin, I. V. Bilych, L. N. Bezmaternykh, and I. A. Gudim, *Fiz. Nizk. Temp.* **36**, 376 (2010) [[Low Temp. Phys.](#) **36**, 296 (2010)].

⁵G. A. Zvyagina, K. R. Zhekov, A. A. Zvyagin, I. A. Gudim, and I. V. Bilych, *Fiz. Nizk. Temp.* **38**, 571 (2012) [[Low Temp. Phys.](#) **38**, 446 (2012)].

⁶B. Luthi, *Physical Acoustics in the Solid State* (Springer, Heidelberg, 2007).

⁷E. A. Masalaitin, V. D. Fil', K. R. Zhekov, A. N. Zholobenko, T. V. Ignatova, and S.-I. Lee, *Fiz. Nizk. Temp.* **29**, 93 (2003) [[Low Temp. Phys.](#) **29**, 72 (2003)].

⁸G. A. Zvyagina, K. R. Zhekov, I. V. Bilych, A. A. Zvyagin, I. A. Gudim, and V. L. Temerov, *Fiz. Nizk. Temp.* **37**, 1269 (2011) [[Low Temp. Phys.](#) **37**, 1010 (2011)].

⁹M. Tachiki and S. Maekawa, *Prog. Theor. Phys.* **51**, 1 (1974).

¹⁰O. Chiatti, A. Sytcheva, J. Wosnitza, S. Zherlitsyn, A. A. Zvyagin, V. S. Zapf, M. Jaime, and A. Paduan-Filho, *Phys. Rev. B* **78**, 094406 (2008).

¹¹A. A. Demidov, I. A. Gudim, and E. V. Eremin, *Zh. Eksp. Teor. Fiz.* **141**, 294 (2012).

¹²A. N. Bogdanov, V. A. Galushko, and V. T. Telepa, *Fiz. Tverd. Tela (Leningrad)* **23**, 1987 (1981); A. N. Bogdanov and V. T. Telepa, *Fiz. Tverd. Tela (Leningrad)* **24**, 2420 (1982).

¹³V. G. Baryakhtar, A. N. Bogdanov, and D. A. Yablonskii, *Usp. Fiz. Nauk* **156**, 47 (1988).

¹⁴V. G. Baryakhtar, A. A. Galkin, A. N. Bogdanov, V. A. Galushko, and V. T. Telepa, *Zh. Eksp. Teor. Fiz.* **83**, 1879 (1982).

This article was published in English in the original Russian journal. Reproduced here with stylistic changes by AIP Publishing.